ANALYSIS AND OPTIMIZATION OF THE TRANSIENT STAGE OF STOPPER-ROD POUR

David D. Goettsch[1], Michael Barkhudarov[2]

[1]General Motors Powertrain
895 Joslyn Avenue, Pontiac, MI 48340-2925

[2]Flow Science, Inc.,
683 Harkle Road, Suite A, Santa Fe, NM 87505

Keywords: Aluminum; Stopper-rod pouring; X-ray radiography

Abstract

Stopper-rod controlled pouring systems offer a simple, efficient method for metal delivery in high production cast lines. However, the raising of the rod from the nozzle creates a complex flow front that may result in air entrainment and oxide film creation that are detrimental to casting quality. Three primary factors that result in defect creation and compromise casting quality are: 1) metallostatic head pressure, 2) shape of the rod, and 3) the speed and height of its removal from the nozzle. Our present work aims to employ numerical modeling to enhance the understanding of this essentially transient flow. The model will then be applied to optimize the process and minimize the potential for such defects. Real time X-ray visualization will be used to validate the results.

Introduction

The quality of a casting is determined in large part by the damage done to the metal during the pouring process. Air entrainment needs to be minimized in the metal delivery system since filters and the gating systems cannot eliminate all the prior damage [1]. The stopper-rod pouring system has many advantages in production over tilt pouring, but it is difficult to reduce the flow rate without entraining air. While it would be optimum to not throttle the rod in the nozzle, this is not practical because of variation in the flow rate accepted by the gating and also different product mix on the line.

The aim of the current work was to perform a detailed experimental and numerical investigation of a production stopper rod and determine a way to minimize metal damage in the throttled condition. The metal flow through the nozzle was examined while the stopper rod was positioned at different heights above the nozzle. A conical design of the rod tip was also investigated. Finally, the effect of different wetting conditions between metal and the surfaces of the stopper rod and nozzle were studied.

Experimental Method

In order to evaluate the effect of the stopper rod movement on the metal flow through a nozzle, a clay-graphite A50 crucible was modified to accept a graphite nozzle. The graphite allowed a detailed view of the aluminum metal front in the nozzle using a 450 kv x-ray source, an image intensifier, and a 720x480 pixels, 30 frames-a-second movie capture card.

A sintered silicon carbide stopper rod was visually centered and seated into the nozzle, while an industrial robot was programmed to raise the rod at a specific speed and height during the tests. A schematic is shown in Figure 1 of the crucible, nozzle and the sintered silicon carbide rod.

A319-aluminum alloy was poured from the crucible at 715°C with an initial head height of 0.165m. Although obstructed by the supporting frame in the x-ray image, the metal stream exiting the nozzle fell freely into a sand basin and did not apply backpressure.

Selected frames from the x-ray videos are shown in Figure 2.
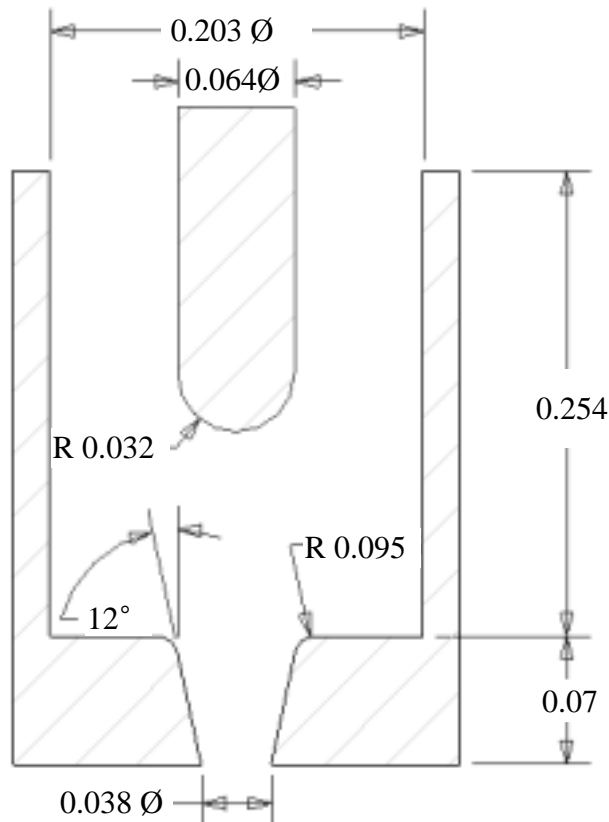
Figure 1. A schematic diagram of the cylindrical crucible, nozzle and stopper rod.

Modeling

Numerical modeling was carried out using the simulation software *FLOW-3D*[®] [2]. Flow was assumed to be axi-symmetric, so the model was reduced to two dimensions – radial and axial. The geometry and flow were represented by a mesh of rectangular control volumes in a cylindrical coordinate system with the axis located at the axis of symmetry of the geometry shown in Figure 1. The computational domain and initial conditions are shown in Figure 3.

The boundary condition at the top of the domain was a fixed pressure head of 0.145m above the upper edge of the domain, which corresponded to the initial condition in the experiment. The experiment showed that the variation of the level of metal in the crucible affected the flow at the nozzle mostly towards the end of the process, when the crucible was almost empty. Therefore, it was deemed a satisfactory approximation to assume the pressure head in the model to be constant. At the bottom, a fixed ambient air pressure was used, equal to 1.013×10^5 Pa.

Numerical tests showed that turbulence did not play a significant factor, so the flow was described with the laminar Navier-Stokes model [3]. Heat transfer was also excluded since no solidification took place in this part of the flow and buoyancy driven flow was negligible. Surface tension proved to be important to capture the flow separation and air entrainment. The nozzle and rod surface were assumed non-wetting with the contact angle of 160 degrees.
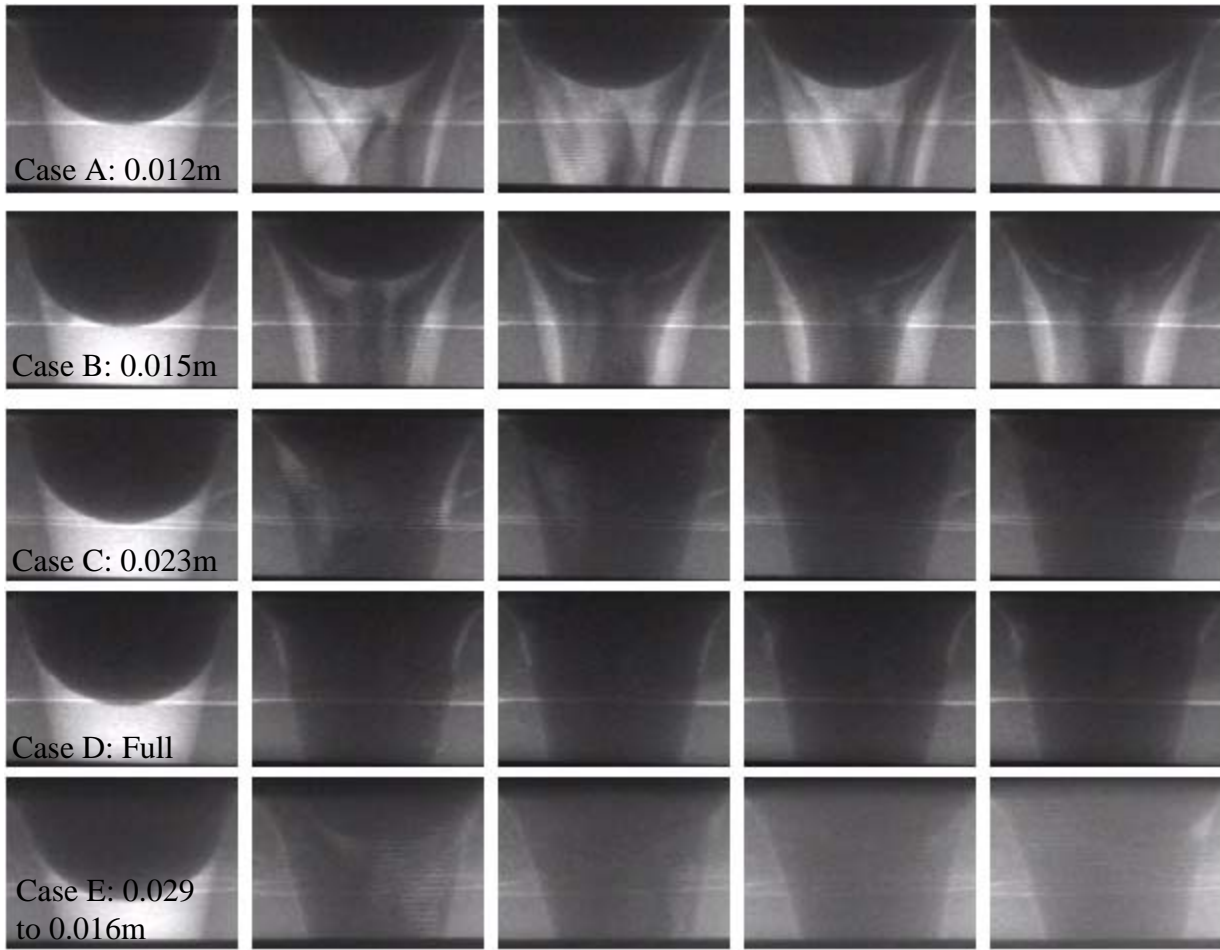
Figure 2. Selected frames from x-ray videos for cases A through E. Frames are 1.0s apart for case A, 0.67s for case B and 0.33s for cases C, D and E.

The inertial properties of air were neglected. The effect of air on the flow was modeled using an adiabatic bubble model [2], where each bubble was characterized by its volume, V, and uniform pressure, P, related to each other according to

$$P=P_0 (V_0/V)^{\gamma} \tag{1}$$

Where P_0 and V_0 are the initial bubble pressure and volume, respectively, and γ is the ratio of the specific heats, equal to 1.4 for air. Bubbles connected to the lower boundary assumed its pressure, irrespective of the bubble volume.

Results

Seven cases were modeled. In four of the cases the rod was lifted from the fully closed position to a height of 0.012m (case A), 0.015m (case B), 0.023m (case C) and fully out of the crucible (case D). The motion of the rod was completed in less than 0.2s, which was much shorter then the time it took to drain the crucible (2 to 6s). Therefore, the numerical model was further

simplified by ignoring the movement of the rod in these four cases. The rod was initialized in the model at the final open position in each of these cases, shown in Figure 3.
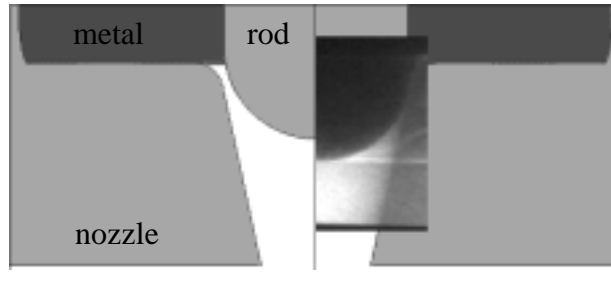
Figure 3. Initial condition of numerical model with overlaid x-ray image. The model of the rod is elevated to its final position, while in the experiment it is initially blocking the nozzle.

In the fifth case, the rod was moved up and then down, attempting to get rid of the air inside the nozzle and achieve a required flow rate. The motion of the rod was important in defining the motion of the air bubbles forming underneath the rod, so it was included in the model by using a moving object model with a time-dependent vertical velocity. The rod moved in a two-stroke cycle with an initial raised height of 0.029m (case E) before moving back down to 0.016m.

A conical rod design was also tested in the numerical model (case F) with respect to the amount of air trapped in the nozzle. The flow conditions were taken from case B, where the rod was initially positioned at the 0.015m height. Finally, case B was modeled with modified wetting condition on the rod and nozzle surfaces (case G). Instead of a non-wetting condition of 160 degrees, used in all other cases, the contact angle for this case was equal to 30 degrees, which corresponds to wetting surface.

The properties of the aluminum alloy used in the simulations are:

Density – 2410 kg/m^3;
Dynamic viscosity – 1.3x10^{-4} Pa-s;
Contact angle - 160° [4,5];
Surface tension coefficient – 0.91 Kg/s.

The simulations were run until a steady-state flow was achieved and the corresponding flow rates are given in Table I. The computed flow rate show good correlation with the average flow rate observed from the experiments. In cases A-D, a steady-state solution was reached well within half a second from the start of the simulation. In cases E, the steady state was delayed by the motion of the rod, and was reached in about 0.8s.

Figure 4 shows the results for cases A-D. The convergence of the metal streams underneath the stopper rod caused an entrapment of air bubbles on the rod surface. These air bubbles could not escape because of the low pressure created as the flow attempts to follow the curvature of the rod. Note also the separation of the flow at the nozzle sidewall. Moving the rod further upwards created a larger opening for the flow. As the flow rate increased, the size of the separation zone at the nozzle wall decreased, but some separation remained even when the stopper rod was completely removed.

X-ray images overlaid on the computational results were taken at times when the observed flow was close to a steady state and are consistent with the computed steady-state flows.
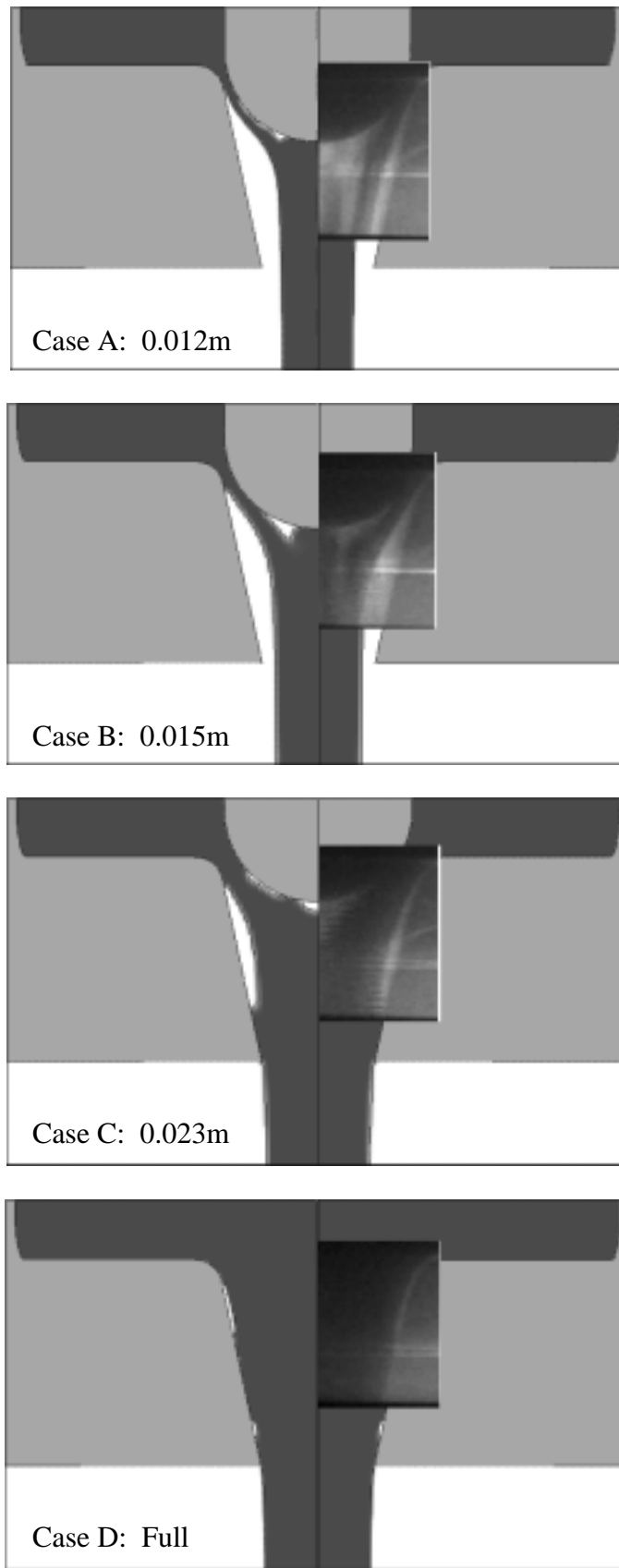
Figure 4. Numerical and experimental results for cases A through D. The flow in the experiment for case A was not quite axi-symmetric because the rod shifted to the left, resulting in a larger opening on its right. This may explain the relatively significant discrepancy in the size of the separation zone.

Table I. Steady state flow rates of observed and simulated rod height cases.

Case	Rod height (meters)	Observed flow rate (kg/s)	Computed flow rate (kg/s)
A	0.012	1.93	2.27
B	0.015	3.00	3.35
C	0.023	5.16	5.09
D	Full out	5.40	5.33
E	0.029 to 0.016	4.06	3.74
F	0.015 (conical tip)	N/A	4.40
G	0.015 (wetting)	N/A	5.06

Figure 5 shows the simulation results for case E at different times. At 0.2s, the flow purged the air bubbles from the nozzle cavity as the rod was lifted to a 0.029m height. After this short purging, the rod was lowered to 0.016m and the flow rate decreased without air entrainment in the steady state. Some bubbles moved up along the side of the rod, but most of the air escaped downward with the metal stream. It took about 0.75s for all air to escape from the nozzle area, which agrees with the observations in Figure 2. A different stopper rod design would be required to reduce the volume of purged air during the transient stage of pouring.

0.0s   0.2s   0.4s   1.0s
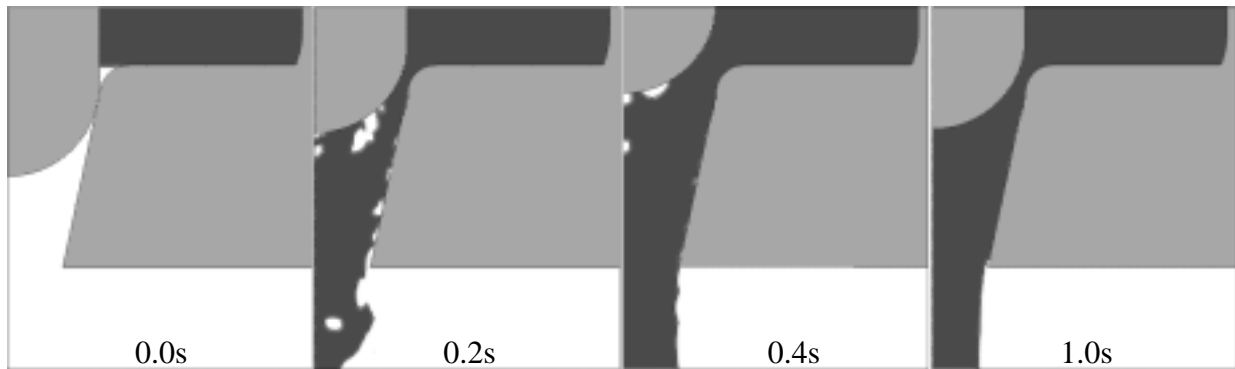
Figure 5. Numerical results for case E were two stage stroke purged bubbles down with the metal stream and up the rod surface at 0.2s. There was no trapped air in the nozzle during the steady state throttled condition.

Cases F and G were modeled only numerically. In case F the hemispherical tip of the stopper rod was replaced with a conical one that matches the draft angle of the nozzle. Case G involved changing the wetting properties of the rod and nozzle surfaces. These variations were easily introduced into the model making it an ideal tool for such studies.

Figure 6 shows results for the conical rod design. There is no flow separation at the wall of the rod, resulting in a continuous flow along the conical tip with no trapped air bubbles. However, an air bubble does get trapped at the nozzle wall, where flow separation still occurs. Compared to the hemispherical design, case B, the amount of trapped air is much smaller, flow is smoother and flow rate higher.
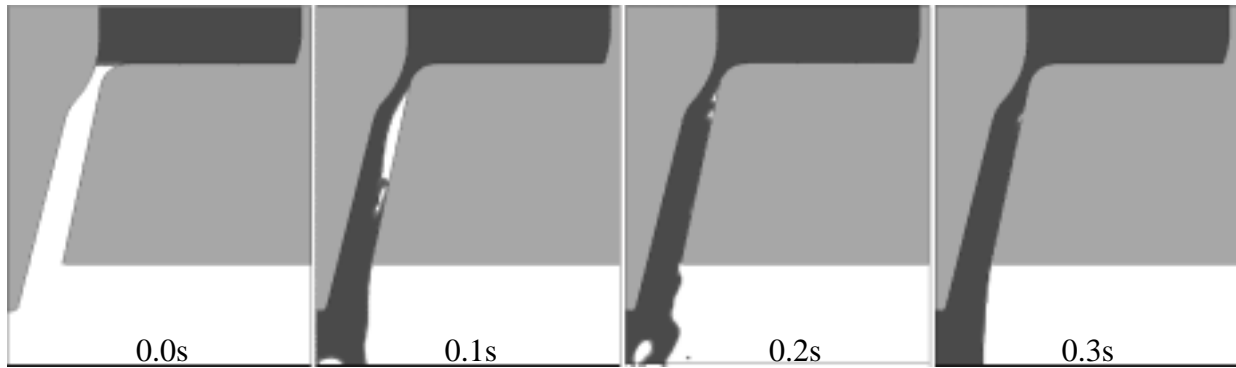
Figure 6. Numerical results for case F were conical rod reduced bubbles trapped at the nozzle wall at the throttled condition.

The most dramatic changes to the flow come from modifying the property of the rod and nozzle walls from non-wetting to wetting, as shown in Figure 7. The advancing metal front formed a concave meniscus, preventing separation and bubble formation during the initial stage of the flow. In the steady state, the nozzle is completely filled with metal. This created a siphon effect and resulted in a 50% higher flow rate than in the non-wetting case B, having the same open area (Table I).
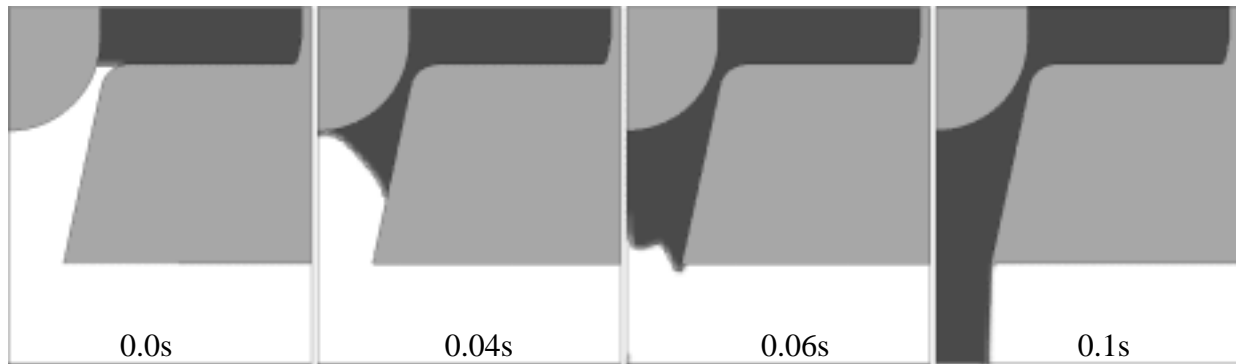
Figure 7. Numerical results for case G were contact angle of 30 degrees inhibited air bubble formation.

Conclusions

An experimental and numerical study of metal flow in a stopper rod pouring system was performed. A range of rod heights and stages were investigated to determine their effect on flow separation and flow rate.

1) Air pockets existed in the steady state during all single stage cases where the rod throttled the nozzle. The void regions were located below the rod and along the nozzle walls with their size diminishing as the rod height increased.
2) A two-stage stroke successfully purged bubbles from the nozzle region and reduced the steady state flow rate. The high stroke stage forced the bubbles out of the nozzle and the bubbles did not form when the rod was lowered back into the nozzle.
3) Numerical simulations of the stopper rod system showed good agreement with experimental data across the range of rod heights. Both the surface tension and bubble pressure proved to be important factors in accurately modeling the flow field.
4) A conical design of the rod reduced the amount of trapped air and increased flow rate.

5) Changing the rod and nozzle wall properties from non-wetting to wetting completely eliminated air entrapment and produced a 50% higher flow rate. Wetting conditions could be modified in a production system by the use of coatings.

Higher flow rates were achieved in cases with little or no air trapped in the nozzle area than in cases with significant flow separation. This can be explained by a siphon effect created by the metal flowing down under gravity. In the absence of air bubbles, a low-pressure region is formed below the rod, increasing the pressure difference across the choke and hence the flow rate.

Acknowledgements

References

1. Campbell J; 1991 *Castings* Butterworth Heinemann.
2. Flow Science, Inc., Santa Fe, New Mexico, www.flow3d.com.
3. G. K. Batchelor, An Introduction to Fluid Dynamics, Cambridge University Press, 1967.
4. K. Landry, S. Kalogeropoulou, N. Eustathopoulos, Mater. Sci. Eng. A254 (1998), 109.
5. W. Laurent, C. Rado, N. Eustathopoulos, Mater. Sci. Eng. A205 (1996), 8.